



Dynamic Properties of Thermally Treated Granite Subjected to Cyclic Impact Loading

Pin Wang¹ · Tubing Yin¹ · Xibing Li¹ · Shuaishuai Zhang¹ · Lv Bai¹

Received: 9 October 2017 / Accepted: 20 September 2018 / Published online: 22 October 2018
© Springer-Verlag GmbH Austria, part of Springer Nature 2018

Abstract

The Earth's deep rock mass is subjected to various complex temperature and stress perturbations. To study the effect of temperature and dynamic disturbance on the damage mechanical properties of these rocks, a series of laboratory tests was carried out by means of a modified split Hopkinson pressure bar system. Specimens were heat treated from room temperature up to a maximum of 800 °C and then cooled to room temperature. During repeated loading tests, the dynamic incident energy was kept constant in each cycle. For samples under the same treated temperature, the dynamic strength and deformation capacity degraded gradually with increasing impact number. Furthermore, rock strength decreased with increasing treated temperature, with the number of impacts before failure reduced accordingly. Since damage can be initiated by thermal treatment and then aggravated by dynamic disturbance, according to the observed decrease in rock strength and increase in strain rate under the different temperature conditions, a temperature of 400 °C was found to be a significant failure threshold. The maximum strain was employed to describe damage evolution during cyclic impact loading, indicating that fatigue damage is gradually accumulated and maintains a three-segment growth with an increase in repeated impacts. Under the coupled effect of temperature and cyclic impact loading, specimens exhibited two different failure modes: split tensile failure and unloading failure. The micro-properties of fracture morphology in granite after different temperature and repeated impact were also discussed in detail.

Keywords Rock dynamics · Thermal treatment · Cyclical load · Impact fatigue · Damage evolution

List of Symbols

SHPB	Split Hopkinson pressure bar
RPC	Reactive powder concrete
BD	Brazilian disc
SCB	Semi-circular bend
SR	Short rod
XRD	X-ray diffraction
ISRM	International Society for Rock Mechanics
SEM	Scanning electron microscope
MTS	Material test system
SRIF	The dynamic strain rate increase factor
v_v	Volume increase rate
V_1	Volume of specimen before thermal treatment (cm ³)
V_2	Volume of specimen after thermal treatment (cm ³)

ε_I	Signal on the incident bar
ε_R	Signal on the reflected bar
ε_T	Signal on the transmitted bar
D	Diameter of the specimen (mm)
L_s	Length of the specimen (mm)
A_e	Cross-sectional area of elastic bars (mm ²)
A_s	Cross-sectional area of the specimen (mm ²)
C_e	Wave propagation velocity in the elastic bars (km/s)
E_e	Young's modulus of elastic bars (GPa)
a_0	Length of initial crack of specimen (mm)
a_c	Critical crack length of specimen failure (mm)
σ_r	Critical stress for fatigue propagation (MPa)
σ_c	Critical failure stress (MPa)
K_I	The stress intensity factor
K_{IC}	The quasi-static fracture toughness
P_1	Force between the specimen and input bar (kN)
P_2	Force between the specimen and output bar (kN)
E_d	The dynamic elastic modulus of the specimen (GPa)
σ_I	The incident stress during cyclic impact (MPa)

✉ Tubing Yin
tubing_yin@mail.csu.edu.cn

¹ School of Resources and Safety Engineering, Central South University, Changsha 410083, China

σ_d	The failure strength during cyclic impact (MPa)
$\dot{\epsilon}_f$	Strain rate during the last impact (m/s)
ρ	Density (g/cm^3)
R^2	Coefficient of correlation
n	Cycle impact number
D	Damage value of specimen
ϵ_{\max}^1	The first impact maximum strain of specimen
ϵ_{\max}^n	Instantaneous maximum strain after n cycles
ϵ_{\max}^N	Ultimate maximum strain under cyclic impact

1 Introduction

For some time, the calculation of structural or rock strength for engineering purposes has been based on structural and material mechanics. Such methods usually assume that the material is a homogeneous continuum, without considering the existence of cracks and defects; as long as the work stress does not exceed the allowable stress, the structure is considered safe (Carroll and Daly 2015). However, with the recent progress in scientific research and the development of engineering practice, it has been proved that the above assumption is not quite correct, with many engineering structures often failing at stresses lower than the determined strength.

In fact, in actual engineering practice, any construction method may bring about different degrees of damage or destruction to the reserved rock mass, which will influence the safety and stability of the project. Most rock failures are not induced by a single load, but are rather caused by fatigue failure due to the repeated action of multiple types of load, such as multiple strikes against targets, the repeated blasting of the engineering rock mass and the destruction of the rock mass by earthquake aftershocks. Based on an understanding of the cyclic loading of the surrounding rocks in the general rock mass, the mechanical properties of rock under static or quasi-static cyclic loading have been studied by both domestic and foreign scholars, with a wealth of research findings published (e.g. Ge et al. 2003; Liu et al. 2014; Sun et al. 2017). For instance, Bagde and Petroš (2009) carried out fatigue tests to investigate fatigue and dynamic energy variation in sandstone and conglomerate. The authors concluded that the development of fatigue failure in these rocks was closely related to their petrographic, physical and mechanical properties, and that micro-fracturing was the main cause of fatigue failure. Ray et al. (1999) examined the relationship between the fatigue life and strain rate of sandstone under three different loading strain rates, finding that the fatigue life of sandstone was lower under a higher strain rate. Liu and He (2012) performed a series of laboratory tests to assess the effects of confining pressure on the mechanical properties and fatigue damage evolution of sandstone samples subjected to cyclic loading. Their results indicated that as the confining pressure increased the axial strain at

failure also increased, suggesting that the level of confining pressure had a significant influence on the cyclic dynamic deformation and fatigue damage of the rock. Li et al. (2003) focused on the mechanical properties of a jointed rock mass subjected to dynamic cyclic loading, finding that the fatigue strength increased with an increase in the dynamic loading frequency. Xiao et al. (2009, 2010) conducted cyclic loading tests on granite from the Heng Yang region of China to find a suitable damage variable to describe fatigue damage in rocks. The authors pointed out that the residual strain method considers the initial damage of the rock and conforms to the three-stage change law of damage accumulation, which is the most ideal method to characterise damage evolution.

However, whereas the above static or quasi-static cyclic loading tests were limited to mechanical responses at low strain rates, in much engineering practice, rock is often subjected to explosions or earthquakes caused by repeated impact. Therefore, an investigation of rock mechanical response under a high strain rate has important practical significance. Lai and Sun (2010) and Wang et al. (2013) investigated the dynamic mechanical behaviour of reactive powder concrete subjected to repeated impact loading. In both papers, the standardised strength of multiple impact compression was defined and the influence of impact times, impact modes and fibre volume fraction on the properties of RPC subjected to repeated impacts was explored. Li et al. (2005) carried out a series of cyclic impact loading tests using a shaped striker in a large-diameter SHPB system to investigate the damage done to granite when subjected to dynamic loading with a relatively low amplitude. The authors concluded that cumulative damage to the rock derived from repeated impact loading depended on either the energy of the external dynamic load or the peak stress of the load with a fixed duration. When the peak stress ranged at between 60 and 70% of the static strength of the rock, the damage generated by each impact was low. However, when the peak stress was close to the static strength, as few as two to three impacts resulted in the total destruction of the rock. Jin et al. (2012) conducted a series of cyclic impact loading tests on sandstone under different static loading conditions. The results of these tests revealed that the level of axial stress had a considerable influence on the resistance capacity of the rock for the same cyclic impact, with the rock resistance capacity the strongest when 22% uniaxial compressive strength was pre-compressed. Wu et al. (2014) and Luo et al. (2015) studied the fatigue behaviour of rock subjected to repeated impact loading by means of an SHPB system equipped with a steel sleeve. Their results indicated that under repeated impact loading, the elastic modulus and the ability of the rock to resist deformation continued to decrease, while the variation in peak strain at each impact increased with the number of impacts. In addition, whereas

the P-wave velocity decreased sharply when the number of impacts was small, this decrease became more gradual as the number of impacts increased.

During the process of deep rock mass mining, the underground rock mass must face not only complex static or dynamic loading disturbances, but also a complex geological environment characterised by high temperatures (Yin et al. 2012; Zhao 2016), water saturation (Zhou et al. 2017a, b) and chemical action (Karfakis and Akram 1993). Engineering rock masses encounter high-temperature environments more frequently, especially during activities such as rock drilling, ore crushing, deep petroleum boring, geothermal energy extraction and the deep burial of nuclear wastes (Heuze 1983; Homand-Etienne and Houpert 1989). At present, a great number of tests have been performed to the mechanical properties of rock under high temperature (Ranjith et al. 2012; Dwivedi et al. 2008; Yin et al. 2018). However, there are also lots of topics in rock mechanical engineering, such as underground coal gasification (Roddy and Younger 2010), volcano stability assessment (Schaefer et al. 2015), and building or tunnel fires (Das et al. 2017); the post-disaster reconstruction, repair, reinforcement and safety assessment also need to consider the changes in the properties of the rock after high temperatures. High temperatures can cause thermal expansion of rock-forming minerals, thermal stresses, and chemical reactions in a rock body and thus produce micro-cracks and damages rock microstructures. After cooling down to room temperature, thermal-induced changes are irreversible to some extent (Hajpál and Török 2004; Tian et al. 2017). Therefore, the mechanical behaviour of rocks after high temperature is also an important aspect for engineering excavation, with many studies examining rock dynamic mechanical properties after thermal treatments (Yao et al. 2016; Fan et al. 2017). Liu and Xu (2013) investigated the effects of temperature and impact loading on the mechanical properties of marble by means of a split Hopkinson pressure bar (SHPB) system. According to their results, the transformation of mineral components and the change in mineral particles were the two main reasons for the observed variation in the dynamic mechanical properties of the marble after heating. Yin et al. (2015, 2016) carried out a study examining the effects of temperature and strain rate on the dynamic tensile properties of Laurentian granite, using Brazilian disc (BD) and semi-circular bending (SCB) testing methods. The test results showed that specimens' physical properties such as density, thermal expansion coefficient and ultrasonic wave velocity were influenced by temperature, while the dynamic tensile strength increased linearly with a rise in the loading rate and decreased with increasing treatment temperature. Zhang et al. (2001) measured the dynamic fracture toughness of Fangshan gabbro and Fangshan marble subjected to high

temperatures by employing a short-rod (SR) specimen in combination with an SHPB system. They concluded that temperature has a limited influence on the dynamic fracture toughness of such rocks within a limited temperature range (up to 330 °C).

Given the existing studies discussed above, the study of rock materials under cyclic loading has thus far mostly focused on their mechanical properties under static or quasi-static levels; research investigating the dynamic response of rock under cyclic impact is rare. Furthermore, none of the above fatigue studies took the thermal effect into account. This is significant, as during the process of damage accumulation in rocks under cyclic impact loading, the effect of high temperatures on crack initiation, as well as on the propagation and coalescence of internal micro-cracks, cannot be neglected. In the present project, the dynamic characteristics of granite under coupled thermal treatment and repeated impacts were studied, with scanning electron microscopy employed to analyse the internal structural damage done to the rock after different high-temperature treatments and repeated impact loading. In addition, rock dynamic properties and damage evolution are also discussed after cyclic impact loading at constant amplitude.

2 Rock Description and Specimen Preparation

2.1 Granite Material

The rock material used in this study was a coarse-grained granite that is widely available in the Changsha area of Hunan province, China. These granite blocks are dark grey in colour, with a highly uniform texture, density (2.65 g/cm³) and compressive strength (126 MPa). Microscopic studies in the form of optical microscopy and X-ray diffraction were performed to provide an insight into rock mineralogical composition and grain sizes, as shown in Figs. 1 and 2. According to these analyses, the granite under study is mainly composed of quartz (46.57%), feldspar (37.95%), mica (9.72%) and montmorillonite (5.76%).

According to the requirements of the rock dynamic mechanical testing procedures suggested by the ISRM (Zhou et al. 2012), the granite was processed into cylindrical samples with a diameter of 50 mm and length/diameter ratio of 1.0. All specimens were carefully ground and polished to a surface roughness of less than 0.02 mm and an end surface perpendicular to its axis by less than 0.001 rad. Before thermal treatment, selected essential physical and mechanical properties of the granite tested under quasi-static loads were obtained, as listed in Table 1.

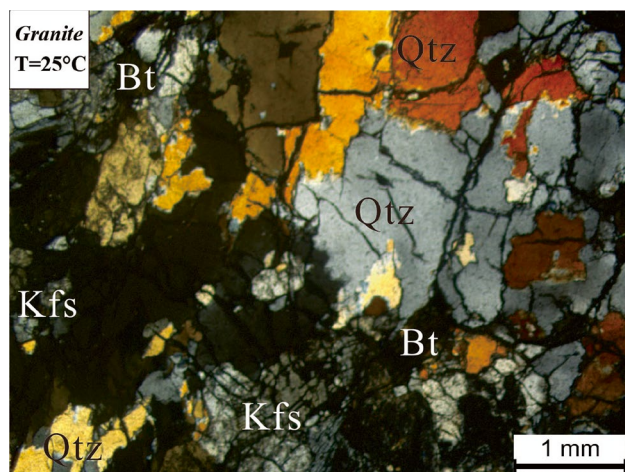


Fig. 1 Photo micrographs of the Changsha granite

2.2 High-Temperature Treatment and XRD Analysis

To simulate the high-temperature environment of rock encountered in engineering practice, specimens were heated in a servo-controlled electrical furnace. Five different temperature levels were selected to produce six groups of samples: five groups were heat treated at 100, 200, 400, 600 and 800 °C, respectively, while one group remained untreated at room temperature for reference. To ensure that the specimens were heated uniformly, the heating speed was set at 2 °C/min; once the specified value was reached, the temperature was kept constant for 2 h. Thereafter, specimens were cooled to room temperature at a lower rate in the furnace chamber to avoid cracking due to thermal shock (Nasseri et al. 2007).

The effect of high-temperature treatment on the characteristics of rock phases is significant, such as mineral species, content, grain size and so on, and the change of phase characteristics is also an important reason for the change of rock mechanical properties. To study the thermal effect on rock mineral components, XRD analysis was conducted for granite samples after different high-temperature treatments. Thereafter, a series of X-ray diffraction patterns of granite and mass fraction of major mineral components after different high temperatures was obtained, shown in Fig. 2. It could be observed from Fig. 2 that the main compositions of granite samples are quartz, feldspar, mica and a small amount of montmorillonite. After different high-temperature treatments, the mineral composition of granite is basically unchanged, but the contents of various minerals changed significantly. The variation of the main mineral mass fraction of granite with increasing temperature is further given in Fig. 3.

It could be observed from Fig. 3 that the quartz is the most important mineral composition of granite, in which the main component is SiO₂. At room temperature (25 °C),

the mass fraction of quartz minerals is 46.57%. With the increase of treatment temperature, some free water inside rock begins evaporating, which resulted that the mass fraction of quartz minerals shows a slight increase at 100 °C. Previous study of Ackermann and Sorrell (2010) and Lima and Paraguassú (2004) has been pointed out that before the temperature of 573 °C, the mineral volume of quartz increases approximately linearly as the increase of treatment temperature. Therefore, pores and micro-defects between some mineral particles will be filled with the expanded quartz mineral, and the internal crystal structure of the rock will be improved (Liu and Xu 2015). However, when temperature rises to 573 °C, the α - β quartz phase transition will occur (Peng and Redfern 2013), which results in the structure of quartz crystal destroyed and the mineral content of quartz shows a rapid decrease during 400–800 °C.

The second main mineral of the granite is feldspar, in which the main composition is that aluminosilicate containing some metal elements Na, K and so on. Under room temperature, feldspar is a kind of brittle material. The effect of heat treatment can make the feldspar exhibit a certain irreversible plastic deformation (Behrmann and Mainprice 1987). Before the treatment temperature of 400 °C, the content of feldspar is basically stable. But when the temperature exceeds 400 °C, the mass fraction of feldspar minerals begins to increase rapidly, which indicates that granite will undergo obvious brittle plastic transition after 400 °C.

Third, the obvious dark mineral on the granite surface is biotite. With the increase of treatment temperature, the crystal structure of biotite is liable to be destroyed due to dehydration, resulting that the mineral content of mica decreases and the color of granite gradually shallower.

Finally, montmorillonite is a layered mineral composed of very fine hydrous aluminosilicate and the water content of montmorillonite varies greatly due to environmental humidity. There are three different heat-absorption valleys in montmorillonite (Grim and Kulbicki 1961): (1) the first heat-absorption valley appears between 80 and 250 °C, in which interlayer water and adsorbed water are removed. (2) The second heat-absorption valley appears between 600 and 700 °C, in which structural water is removed. (3) The third heat-absorption valley appears between 800 and 935 °C, in which crystal structures will be totally destroyed. However, because of the low content of montmorillonite in granite samples used in this paper, the variation of mass fraction of montmorillonite is not obvious after experiencing different temperatures.

2.3 Surface Color and SEM Observation

To examine the effect of thermal treatment on the macro-features and microstructure of the rock specimens, samples subjected to the different high-temperature treatments were

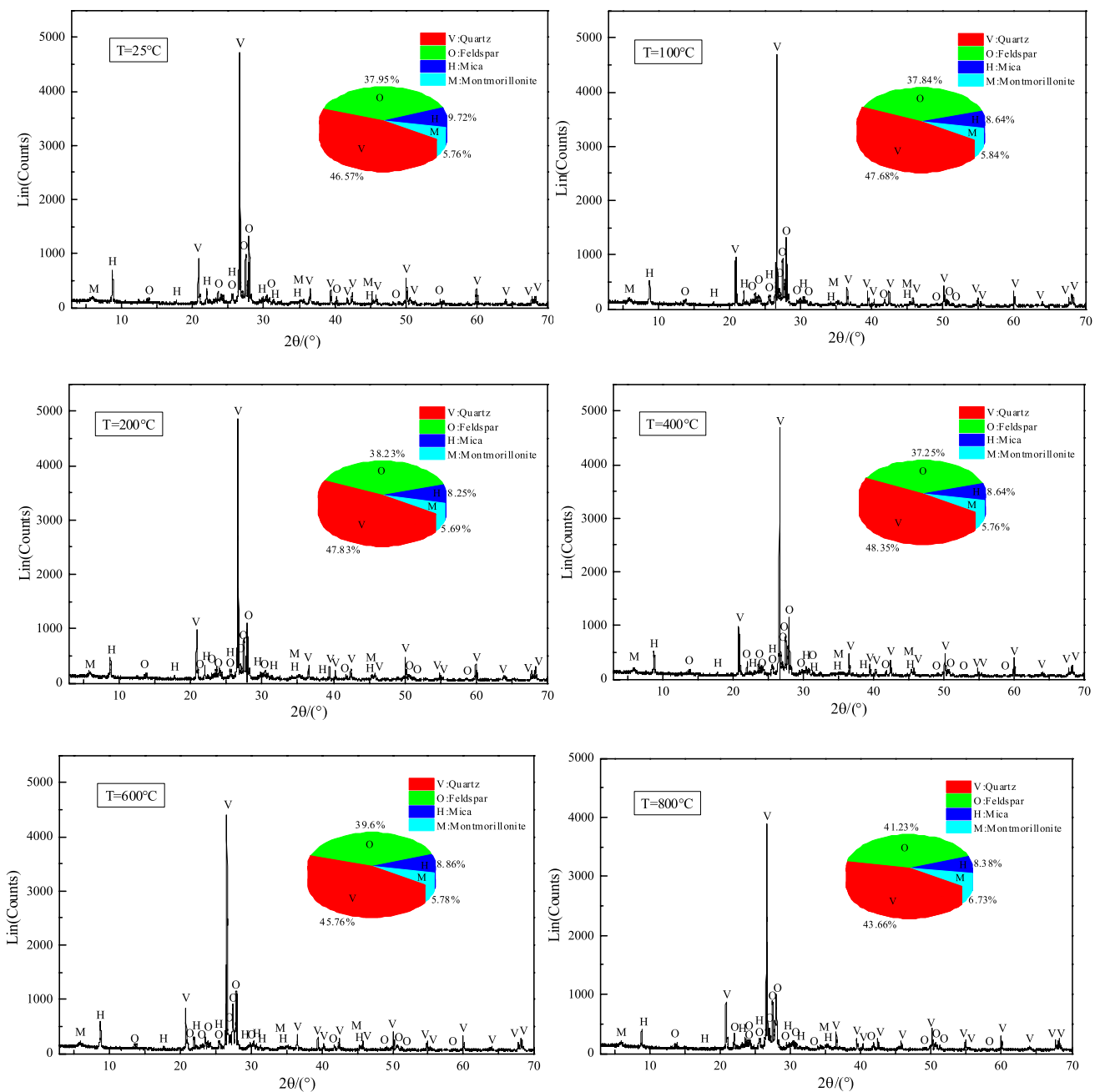


Fig. 2 X-ray diffraction patterns of granite after different high-temperature treatments

Table 1 Physical and mechanical properties of granite at normal temperature (25 °C)

Specimen	Density (g/cm ³)	P-wave velocity (m/s)	Young’s modulus (GPa)	Poisson’s ratio	Tensile strength (MPa)	Compressive strength (MPa)
Granite	2.65	4744.34	23.7	0.21	8.6	126

photographed and scanned, respectively, using a Leica camera and scanning electron microscope (SEM), as shown in Fig. 4.

As can be observed from Fig. 4, temperature had a significant influence on the appearance and internal structure of the tested granite rock specimens. Below 200 °C, the granite

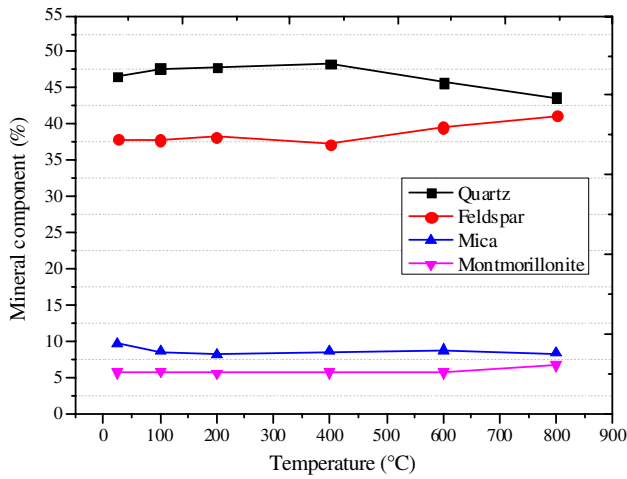


Fig. 3 Variation of the main mineral mass fraction of granite with increasing temperature

was dark grey in colour, with many black spots scattered on the sample surface. At lower temperatures, the internal structure of the granite was compact and smooth with no obvious cracks. A visible intergranular crack first appears in rock when temperature rises to 200 °C. With an increase in treatment temperature, the black spots gradually faded and the samples changed in colour from dark grey to yellow; a slight expansion in volume was also apparent. The main reason for this colour change is likely mineral dehydration and chemical reaction, since the black spots are mainly composed of biotite, whose crystal structure can be easily destroyed by dehydration (Liu and Xu 2015). When the temperature was increased to 400 °C, although the specimen’s appearance remained intact, a number of wider intergranular fractures were found between mineral grains, likely due to free water evaporation and the differential thermal expansion of mineral particles. When the temperature was increased to above 600 °C, rock volume expansion was noticeable and the specimen produced a clear and crisp sound after only a

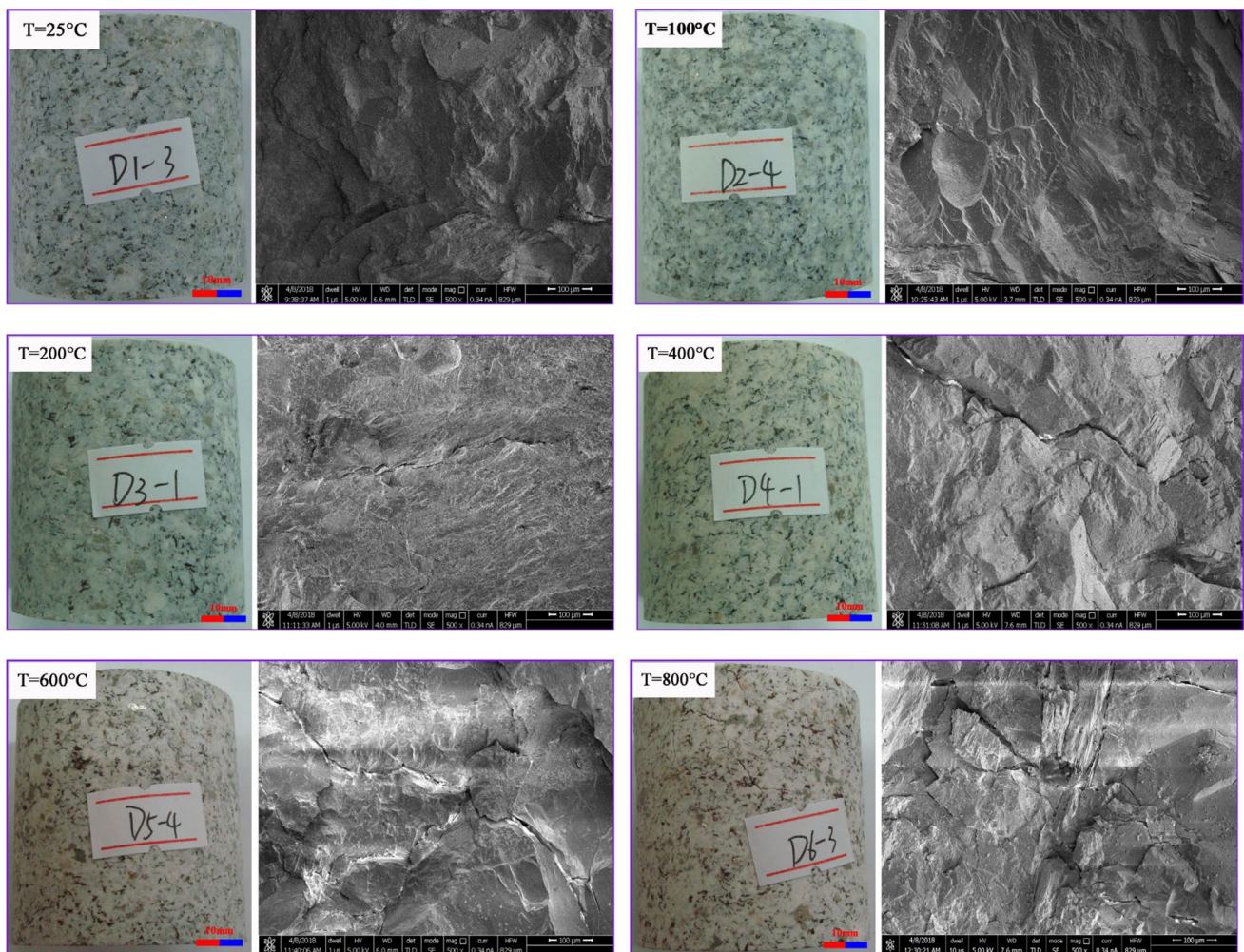


Fig. 4 Photographic and SEM images of granite specimens after different high-temperature treatments

slight collision. At 800 °C, the specimen colour was canary yellow, the rock volume was obviously enlarged and a number of transgranular fractures were found after surface and SEM observations. These features indicate that the highest temperature treatment destroyed the internal structure of the rock, with damage gradually accumulating and eventually resulting in the propagation of macro-cracks.

2.4 Variation in Volume, Porosity and P-Wave Velocity

Thermal expansion is the tendency of material to change in volume or length in response to a change in temperature. However, after high-temperature treatment above 400 °C, due to the uneven thermal expansion of rock mineral particles and the inherent anisotropy of rock, the volume will be greatly changed with extremely random shapes. Therefore, change of rock volume measured by the caliper method will produce a larger error. According to the ISRM's (Franklin et al. 1979) suggested methods for rock characterization, testing and monitoring, it will be more reasonable to measure the volume of a rock sample before and after high temperature by water displacement method with rock samples coated in wax, and its bulk volume determined from the water volume displaced by the coated sample, corrected for the volume of coating material. Thereafter, the variation of volume of a specimen before and after thermal treatment can be easily obtained, represented as volume increase rate (Tian et al. 2014):

$$v_v = \frac{V_2 - V_1}{V_1} \times 100\%, \tag{1}$$

where V_1 and V_2 are the volume of a specimen before and after thermal treatment, respectively.

Figure 5 shows the variation of rock volume increase rate along with the temperature, indicating that the volume keeps a continuous increase with increasing temperature, and the evolutionary process can be divided into three stages. In the first stage, from 25 to 100 °C, rock volume shows an obvious increase, indicating that the mineral particles have been widely expanded. In the second stage, from 100 to 400 °C, the volume increase rate slows down but also maintains steady growth. The main reason causing this phenomenon might be that the expansion rate of mineral particles is small and the new cracks have not been widely formed at this stage. In the third stage, from 400 to 800 °C, rock volume increase rate is steep, which can be explained by the increase in both number and width of the thermally induced microcracks with the heating temperature (Nasseri et al. 2007). For example, when temperature increased to 800 °C, the volume of rock increased by 2.65% compared with that under normal temperature. Although this is a very small change, it can

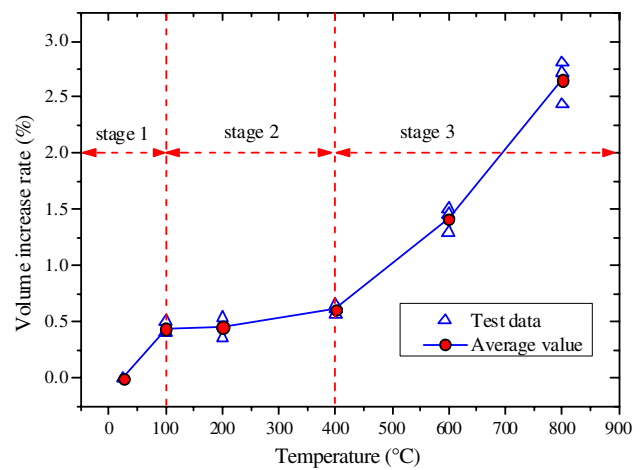


Fig. 5 Relation between volume increase rate and temperature

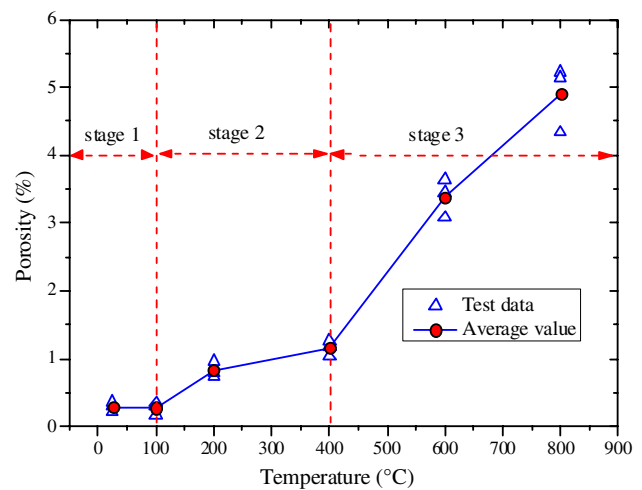


Fig. 6 Variation of rock porosity with the increase of temperature

also indicate that the effect of high temperature causes an irreversible deformation of the rock.

Porosity is one of the most important physical characteristics governing the mechanical resistance and density of rocks. The larger porosity indicates that the rock structure is less dense. The porosity characteristics of the samples after thermal treatment were tested using an AutoPore IV 9500 automatic mercury injection apparatus. Figure 6 shows the variation of rock porosity with the increase of treatment temperature. It could be observed that granite porosity has three stages that vary with the increase of treatment temperature. At the temperature range from 25 to 100 °C, due to the evaporation of free water inside the rock, pores and micro-defects between some mineral particles were exposed. But due to the expansion of quartz mineral particles, some original and newly exposed fissures will be tightly compacted, which resulted that the porosity of rock shows a slight decrease.

Combining with the SEM observation results of granite after different high temperatures, it could be observed that with the increase of treatment temperature, the size of intergranular cracks increases gradually, and some transgranular fractures could be found at the temperature of 600 °C, which resulted that the porosity of rock presents a rapidly increase. But the increase rate of porosity is different during the two stages before and after 400 °C, which might be due to greater damage of transgranular fractures to the rock than the intergranular crack.

The P-wave velocity of granite sample was measured by ultrasonic pulse transmission technique; the results can be shown in Fig. 7. It could be observed that the evolution process of the P-wave velocity can also be divided into three stages and the temperature ranges at each stage is the same as the evolution of rock volume increase rate. Below 100 °C, there is an obvious increase in P-wave velocity from 4744.34 to 5177.69 m/s, with an increase rate of 9.13%. The main reason for this phenomenon is probably due to the evaporation of free water inside the rock and the expansion of mineral particles, which resulted that the inner pores of the rock are filled and the rocks are more compact. Within the temperature range of 100–400 °C, strongly bound water and constitution water gradually escaped, which resulted in the internal structure of rock being no longer dense; thus,

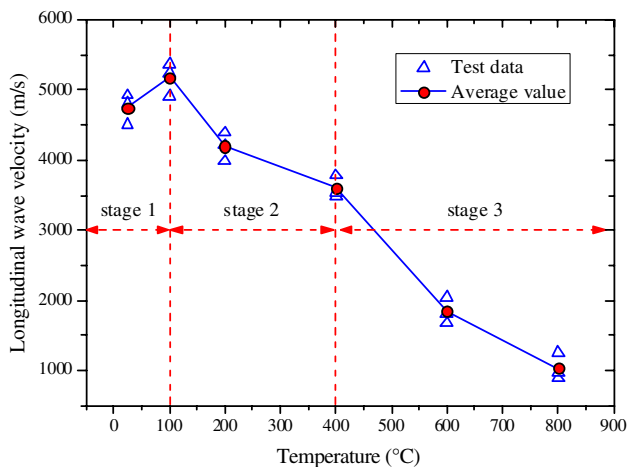


Fig. 7 Variation in longitudinal wave velocity vs. temperature

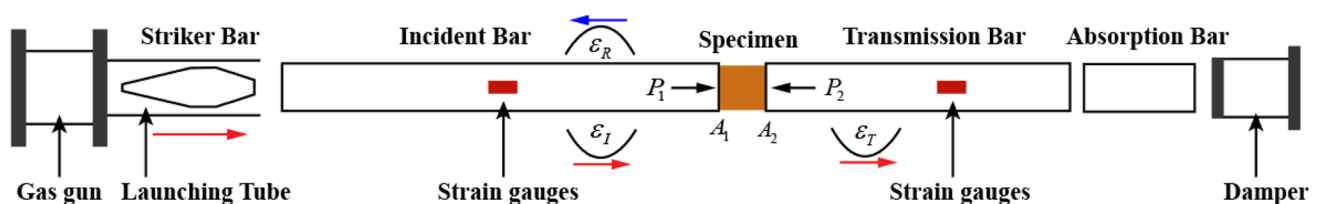


Fig. 8 Schematic of the split Hopkinson pressure bar system

the P-wave velocity has undergone a slow decline. When temperature reaches to 400 °C, there will be obvious structural thermal stress inside the rock. With the increase of temperature, the influence of the thermal stress has become more and more remarkable and the internal cracks accumulate constantly. Especially when it exceeds 800 °C, the P-wave velocity of the granite rock was only about 21.8% of the velocity under the initial temperature 25 °C. This large decrease in the P-wave velocities implies that a great many of thermal cracks and damage must have been induced in the rocks by high temperature.

In summary, the variation in the above three physical parameters all indicate that the heat treatment causes permanent damage to the rock.

3 Test Apparatus and Scheme

3.1 Split Hopkinson Pressure Bar System

Repeated impacts were carried out using an improved split Hopkinson pressure bar (SHPB) device with a specially shaped striker (Li et al. 2000), comprising a gas gun, launching tube, cone-shaped striker, incident bar, transmission bar and absorption bar (Fig. 8). All of the elastic bars were made of maraging steel with a high yield strength of 800 MPa, density of 7810 kg/m³ and elastic modulus of 250GPa; the lengths of the incident bar, transmission bar and absorption bar were 2000, 1500 and 500 mm, respectively. This testing system has the advantage of being adapted for high strain rate loading on heterogeneous brittle materials, with the specially shaped striker eliminating the high-frequency oscillation of the stress waves in the dynamic tests and achieving half sine stress wave loading with a constant strain rate (Zhou et al. 2011; Zhang and Zhao 2014).

During the dynamic tests, granite samples were sandwiched between the incident bar and the transmission bar, with grease coated on both ends of the specimen to ensure good contact between specimen and bars. The striker bar was then shot from a high-speed gas gun, with the velocity or incident energy controlled by both adjusting the position of the striker in the launch tube and the gas pressure, and thereafter impacted on the free end of the incident bar.

Meanwhile, a longitudinal compressive pulse was produced and propagated from the incident bar to the specimen. Due to the difference in wave impedance between the specimen and the elastic bar, the incident pulse (ϵ_I) was partly transmitted (ϵ_T) and partly reflected (ϵ_R). Two strain gauges were fixed to the incident bar and transmission bar, and the mechanical properties of the specimen were calculated via the analysis of the voltage in the strain gauges. According to one-dimensional stress wave theory, values of $\sigma(t)$, $\epsilon(t)$ and $\dot{\epsilon}(t)$ can be calculated using the following formulae:

$$\sigma(t) = \frac{A_e}{2A_s} E_e (\epsilon_I + \epsilon_R + \epsilon_T), \tag{2}$$

$$\epsilon(t) = \frac{C_e}{L_s} \int_0^t (\epsilon_I - \epsilon_R - \epsilon_T) dt, \tag{3}$$

$$\dot{\epsilon}(t) = \frac{C_e}{L_s} (\dot{\epsilon}_I - \dot{\epsilon}_R - \dot{\epsilon}_T). \tag{4}$$

In Eqs. (2), (3) and (4), A_s and A_e , respectively, represent the cross-sectional areas of the specimen and the bar; L_s is the length of the specimen; C_e and E_e , respectively, represent the longitudinal wave velocity and Young’s modulus of elastic bar; and ϵ_I , ϵ_R and ϵ_T , respectively, represent the incident, reflection and transmission strain of the bar.

3.2 Measurement Principles

In the static fracture of brittle materials, the Griffith theory considers that for a material with an initial crack a_0 , it is safe and reliable to work at the static level as long as the working stress σ is less than the critical stress σ_c ; brittle fractures can only occur when $\sigma = \sigma_c$ or $K_I = K_{IC}$ is applied, as shown in Fig. 9. However, if the material is subjected to an alternating stress whose value ranges between σ_f and σ_c , the initial crack a_0 will expand slowly and the component will be subject to fatigue failure when the crack length reaches a_c . Only when the stress amplitude is below a certain value of σ_r will fatigue failure not occur under cyclic loading (Lajtai 1971).

Based on the theoretical analysis of a static fracture proposed by Griffith, Li et al. (2014) stated that for a crack of definite length and subject to either dynamic or static loading, a critical stress threshold exists that is inversely proportional to crack length, with the dynamic value larger than that for the static condition. Considering the attenuation of stress waves and the energy dissipation in rock under various loading conditions, the authors proposed a threshold of energy loading density for dynamic cumulative damage. When the energy density decreases to a certain value, the harmonic of any frequency in the loaded stress wave will not interact with any crack in the rock, and all cracks in the rock will not be extended. Therefore, stress waves of this strength

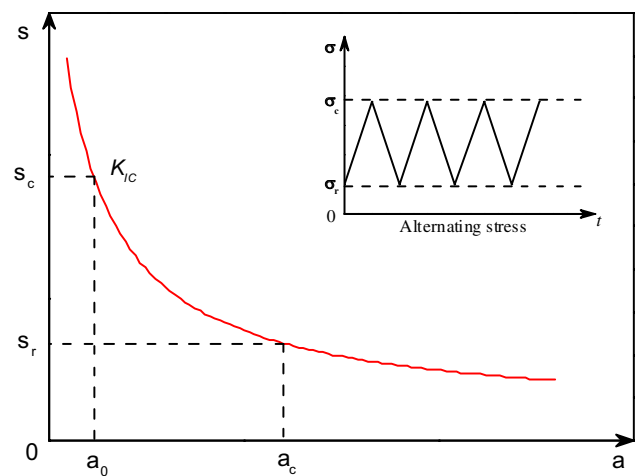


Fig. 9 Schematic diagram of the Griffith crack propagation theory

will not cause damage to the rock. When the energy density of the stress wave reaches its threshold, the crack develops at high speed and the rock will be destroyed by a single impact. Only when the stress wave energy is between the two critical values will each load of the stress wave cause damage to the rock; in this case, cracks propagate at low speed and cyclic loading subjects the rock to gradual damage.

3.3 Laboratory Testing Procedures

3.3.1 Static Compression Tests

Prior to the dynamic fatigue tests, initial granite damage characteristics caused by heat treatment were studied, with static loading tests performed using an MTS hydraulic servo-control testing machine. A constant loading rate of 200 N/s was selected for all tests following the method suggested by the ISRM (1978). The resulting stress–strain curves of granite specimens treated under the six different temperatures are shown in Fig. 10.

It could be observed from Fig. 10 that temperature has a great influence on the static strength of the tested granite. The granite sample heated at 100 °C was found to be strengthened, likely due to free water evaporation, mineral particle expansion and the formation of no new cracks, which led to an increase in specimen compactness. When the treatment temperature rose to 200 °C, the rock particles were sufficiently enlarged to produce tiny new cracks and/or growth in existing primary micro-cracks, resulting in a sharp decrease in granite strength. At 200–400 °C, continued particle expansion increased the porosity of the rock, although due to the anisotropy of these particles, thermal stress was generated, resulting in slow variation in strength and strain. At high temperatures (exceeding 600 °C), the rocks were severely damaged; some mineral particles began to melt and

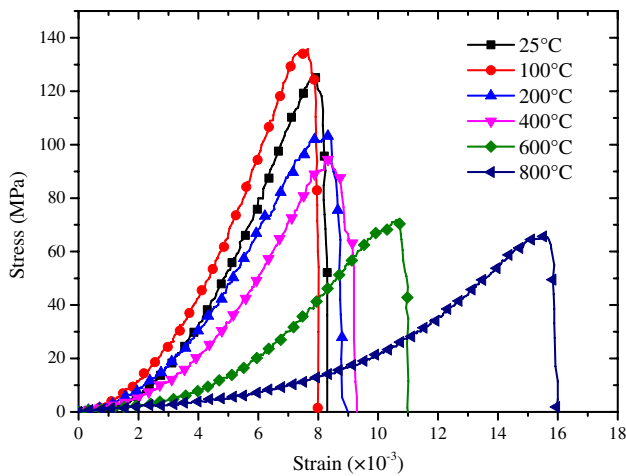


Fig. 10 Static compressive stress vs. displacement for specimens treated under different temperatures

decompose, resulting in rapid decreases/increases in rock strength and strain.

3.3.2 Dynamic Pre-impact Tests

As described in Sect. 3.2, the amplitude of the stress wave plays a decisive role in fatigue tests. When the incident energy is too low, cyclic loading will not cause damage to the rock mass (Bagde and Petros 2005; Li et al. 2005). However, when the incident energy is too high, a single impact will result in the failure of the rock. In the present study, due to their treatment at different temperatures, the specimens suffered various degrees of thermal damage and thus also varied in peak strength. To ensure that all samples were subjected to repeated impact at low constant stress until failure, a number of pre-impact tests were conducted. Two conditions had to be satisfied: first, the incident stress must reach the damage threshold of the rock under normal temperatures; and second, the granite sample must be able to withstand at least two impacts after treatment at 800 °C.

According to the static loading tests described in Sect. 3.3.1, after thermal treatment at 800 °C the static compression strength of the granite is decreased by 50% compared to that at room temperature. Therefore, by adjusting the gas pressure and the position of the striker in the launch tube, a series of pre-impact tests were conducted on samples after heat treatment at 800 °C. Figure 11 presents three single-impact stress–strain curves recorded at three different gas pressures of 0.4, 0.5 and 0.55 MPa, respectively. Thereafter, the fractured state of the rock after different single impact could be observed, as shown in Fig. 12. It could be observed from Fig. 12a that under the gas pressure of 0.45 MPa, intact specimen without obvious cracks can be found. When the impact gas pressure increased to 0.55 MPa, specimen was totally destroyed, as shown in

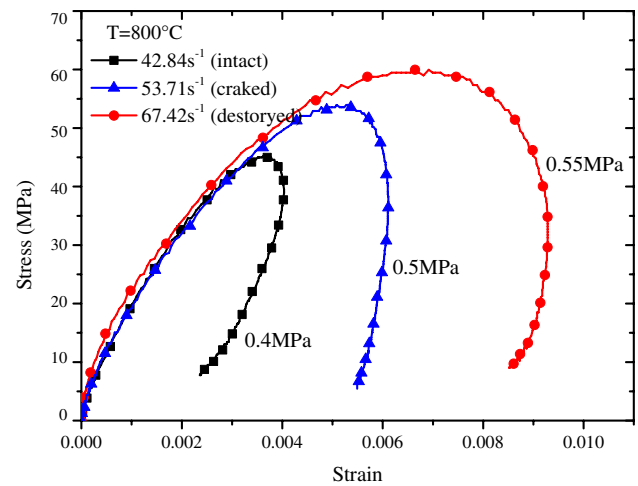


Fig. 11 Stress–strain relationship of Changsha granite for a single impact

Fig. 12b. Only after the single impact with gas pressure equal to 0.5 MPa, although obvious cracks were found in the surface of the specimen, its whole structure remained intact (as shown in Fig. 12c, d), indicating that the granite rocks under study are able to withstand at least two shocks under these conditions. Therefore, we chose a gas pressure of 0.5 MPa as the constant amplitude cyclic loading pressure, with the amplitude stress set at 180 MPa and the incident energy at 140 J.

3.3.3 Repeated Impacts with Constant Amplitude

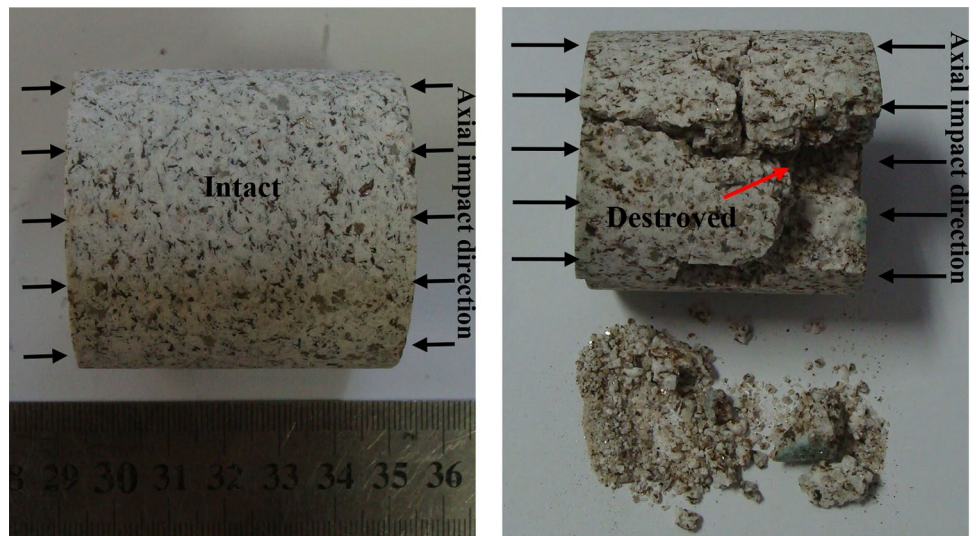
Figure 13 displays an overlay chart of the typical waveform recorded during the cycle impact tests. It can be observed from this figure that the incident wave is essentially coincident in each impact cycle, indicating that constant amplitude cyclic loading has been realised. With an increase in the number of cycles, the amplitude of the transmitted wave becomes higher and higher, and its reach time appears earlier, while the reflected wave exhibits the opposite variation. The main reason for this phenomenon is likely that the accumulation of internal damage under cyclic loading resulted in an increase in rock porosity and wave impedance. Furthermore, the figure also reveals that whereas the transmission and reflection waves in the first few cycles are relatively stable and exhibit little variation, the transmission wave associated with the last impact is markedly increased, indicative of potential mutation failure.

4 Experimental Results and Discussion

4.1 Dynamic Stress Equilibrium

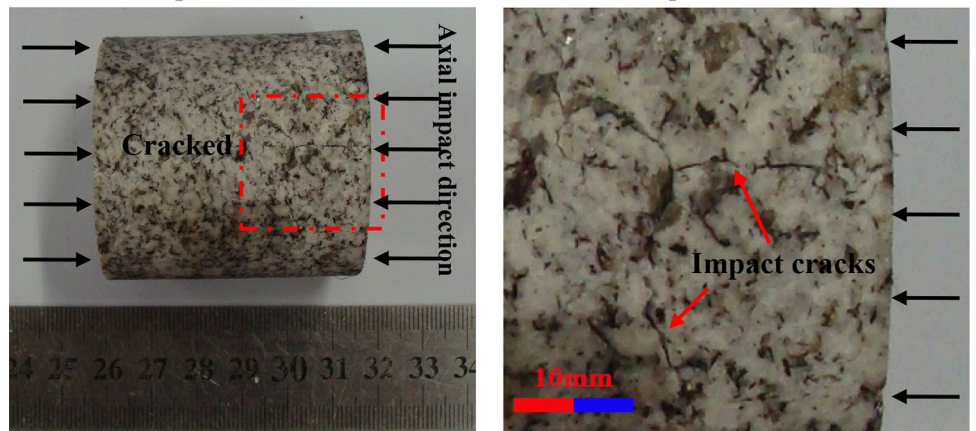
To ensure that the stress inside the specimens was evenly distributed and that the quasi-static equation could be

Fig. 12 Specimen failure image after single impact with different amplitude ($T=800\text{ }^{\circ}\text{C}$)



(a) Gas pressure=0.45MPa

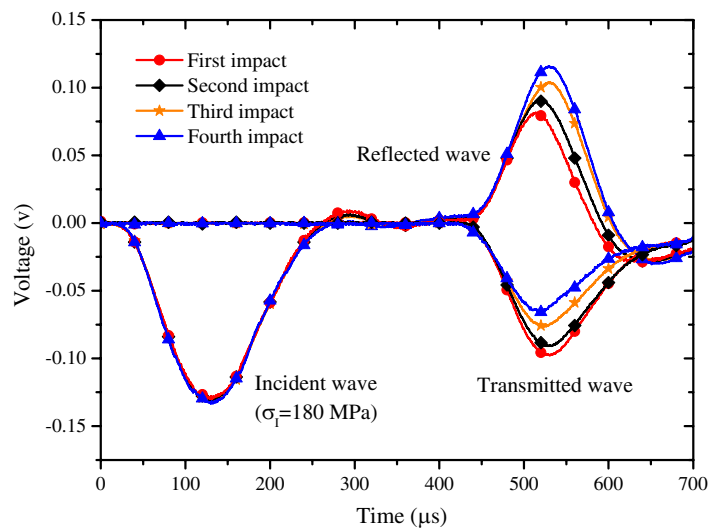
(b) Gas pressure=0.55MPa



(c) Gas pressure=0.5MPa

(d) Local magnified view of (c)

Fig. 13 Variation in stress waves during cyclic impact loading ($T=25\text{ }^{\circ}\text{C}$)



employed to determine the dynamic compressive strength of the rock, dynamic equilibrium verification was necessary (Chen et al. 2009). In the present work, a cone-shaped striker was utilised as a pulse-shaping device, as employed successfully elsewhere (Zhang and Zhao 2014). The loading forces on both ends of the sample are obtained via the following formulae:

$$P_1 = E_e A_e [\varepsilon_I(t) + \varepsilon_R(t)], \quad (5)$$

$$P_2 = E_e A_e \varepsilon_T(t), \quad (6)$$

where E_e and A_e are the elastic modulus and the cross-sectional area of the bar, respectively; and ε_I , ε_R and ε_T , respectively, represent the incident, reflection and transmission strain of the bar.

Figure 14 shows the time-varying forces acting on both ends of the specimen during a typical test, as calculated using Eqs. (5) and (6). It can be seen from this figure that the measured waveform essentially eliminates the wave oscillation caused by stress–dispersion, resulting in a half sine stress wave with an approximate platform on the reflection wave, which indicates that constant strain rate loading has been achieved. The dynamic forces on both sides of the specimen are in a state of balance, as the sum of the incident (In) and reflected (Re) stress waves is absolutely equal to the dynamic force transmitted on the other side, that is, $P_1 = P_2$, and the axial inertial effect can be neglected in the dynamic tests. In the present study, the dynamic force balance was thus checked for all tests.

4.2 Dynamic Properties of Granite Subjected to Repeated Impacts

After a series of cyclic impact loading tests, rock damage accumulated gradually and fatigue failure finally occurred. Selected mechanical parameters and test results for the

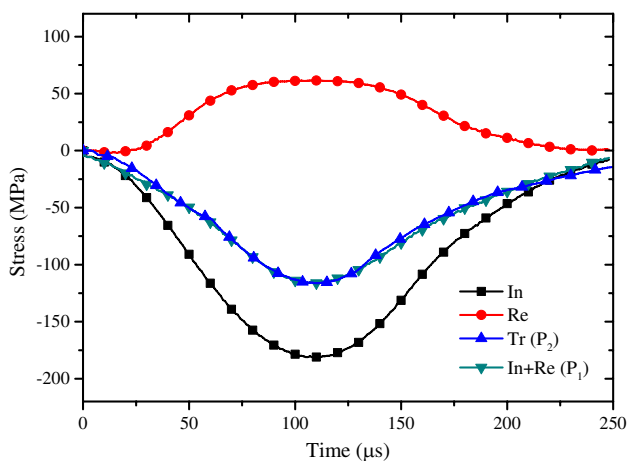


Fig. 14 Dynamic force balance check for a typical specimen (D1-1)

Changsha granite under repeated impacts are presented in Table 2, in which E_d is the dynamic elastic modulus measured at the last impact (determined based on the slope between 40 and 60% of the compressive strength of the increasing stress–strain curve), σ_I and σ_d are, respectively, the incident stress and the failure strength of the rock, and $\dot{\varepsilon}_f$ represents the strain rate during the last cycle. Selected representative stress–strain curves corresponding to the granite rock specimens tested at the six temperature levels and different impact cycles (as obtained from the SHPB experiments) are shown in Fig. 15. The Arabic numerals are used to indicate the cycle loading numbers.

As can be observed from Fig. 15, the stress–strain curves of the specimens subjected to each of the different high-temperature treatments are almost identical in shape at the beginning of the rising phase. Due to the high strain rate of impact loading, the micro-fracture compaction stage does not appear, with a convex curve apparent instead. In addition, owing to the relatively low constant amplitude of cyclic loading, the stress–strain curve after the highest peak rebounds immediately, with specimens maintaining their integrity after the first few shocks. However, with an increase in treatment temperature and after repeated impacts, the residual strain increases and the rebound phenomenon is gradually weakened. For treatments at or exceeding 600 °C, a platform appears in the stress–strain curve, indicating rock transformation from brittle to plastic. Similar results were observed by Shan et al. (2000) and Zhou et al. (2014), who studied the mechanical properties of granite under dynamic compression using the split Hopkinson pressure bar technique. Their results showed that with an increase in the strain rate, the post-peak deformation of the dynamic stress–strain curve gradually changes from elastic to ductile and the stress–strain curves exhibit three different stages: elastic rebound, brittle drop and ductile deformation.

Figure 16 shows the variation in fatigue strength of the specimens tested under different temperatures and cyclic impacts. In all temperature segments, specimen strength continues to decrease with an increasing number of repeated impacts. However, at 25 °C a somewhat different pattern is apparent, with rock strength slightly increased during the first one or two cycles. There are two possible reasons for this increase: first, the granite specimens contain a number of pre-existing cracks, which after the first few loads are compressed, results in the rock becoming more dense; and second, the rock under study is rate sensitive. Many researchers have argued that under high loading rates, the stress reaches a higher level before the initial cracks are aggregated; this requires additional cracks to consume the external force, which in turn leads to an increase in the compressive strength of the rock (Zhao and Li 2000).

A second interesting phenomenon apparent in Fig. 16 is that at low treatment temperatures (below 400 °C), the first

Table 2 Mechanical parameters and test results for granite subjected to repeated impacts

No.	<i>D</i> (mm)	<i>L</i> (mm)	ρ (g/cm ³)	<i>E_d</i> (GPa)	σ_I (MPa)	σ_d (MPa)	$\dot{\epsilon}_f$ (m/s)	Cycles
D1-1	50.30	49.13	2.647	30.58	183	89.27	45.08	13
D1-2	50.32	49.11	2.644	35.22	176	84.33	43.25	13
D1-3	50.28	49.12	2.650	33.05	185	93.54	47.22	12
D2-1	50.57	49.18	2.625	36.84	177	106.87	54.38	15
D2-2	50.01	49.13	2.617	32.47	176	103.41	48.59	13
D2-3	49.98	49.12	2.624	30.46	167	99.76	49.29	14
D3-1	49.91	49.16	2.615	19.16	175	75.33	50.21	10
D3-2	49.91	49.14	2.606	22.33	184	77.12	51.37	11
D3-3	50.23	49.12	2.587	18.97	173	83.44	48.33	11
D4-1	50.57	49.19	2.613	10.49	190	53.21	57	7
D4-2	50.55	49.16	2.623	13.23	182	51.94	57.73	8
D4-3	49.44	49.15	2.598	11.55	177	47.66	52.10	9
D5-1	49.45	49.19	2.601	10.04	172	33.21	60.72	6
D5-2	49.44	49.22	2.593	12.45	169	39.32	58.73	4
D5-3	50.35	49.29	2.589	9.67	176	30.44	60.42	6
D6-1	50.39	49.52	2.570	4.13	180	22.06	70.22	3
D6-2	50.31	49.51	2.553	6.32	178	29.54	58.24	1
D6-3	50.48	49.50	2.560	4.44	172	23.50	67.24	2

few shocks do not significantly reduce rock strength; damage evolution instead exhibits a slow accumulation until a sudden increase, with the rocks ultimately subject to mutation failure during the final cycle. In contrast, when the temperature exceeds 400 °C, damage accumulation increases almost linearly and rock strength decreases linearly with an increase in impact cycle number. Thus, 400 °C can be seen as a temperature threshold below which thermal damage is decreased, but above which the granite is seriously damaged by heat treatment.

4.3 Deformation and Damage Characteristics

The strain rate indicates the difficulty of rock deformation during stress loading, which is in turn closely related to treatment temperature and rock loading conditions, as shown in Fig. 17. Analysis of this figure reveals that at all temperature stages, the dynamic loading strain rate increases continually with an increase in impact number, indicative of fatigue crack propagation and the gradual accumulation of rock damage under repeated impacts. The relationship between strain rate and repeated impact number can thus be described by a linear equation, for which the best-fit line is plotted in Fig. 17 and the fitting equations listed in Table 3.

From Table 3 it is clearly apparent that the slope of the relationship equation not only indicates the increase in the dynamic strain rate with an increasing number of impacts, but also increases with treatment temperature, as fitted via the following equation:

$$SRIF = 1.279 + 0.0052e^{T/151.19} \quad R^2 = 0.955. \quad (7)$$

Here, SRIF is the dynamic strain rate increase factor; its fitting curve with temperature is displayed in Fig. 18. The variation in SRIF with treatment temperature is characterised by slow growth between 25 and 400 °C, and a sharp increase when the temperature exceeds 400 °C. As the strain rate also indicates the extent of rock damage, the observed rapid increase in the strain rate at temperatures above 400 °C confirms that the latter figure can be seen as a significant sensitivity threshold.

As the maximum strain of the tested granite rock increases with the number of repeated impacts, the former can also be used to describe the damage evolution process after each impact. The calculating formula is expressed as follows:

$$D = \frac{\epsilon_{max}^n - \epsilon_{max}^1}{\epsilon_{max}^N - \epsilon_{max}^1}, \quad (8)$$

where ϵ_{max}^1 , ϵ_{max}^n and ϵ_{max}^N are the first impact maximum strain, instantaneous maximum strain after n cycles and ultimate maximum strain, respectively.

Figure 19 illustrates the damage evolution of thermally treated granite subjected to repeated impacts. Analysis of this figure reveals that specimen damage is characterised by three stages at temperatures below 400 °C, including an initial stage, stable development stage and sharply increasing stage. In contrast, at treatment temperatures greater than 400 °C a large number of cracks are generated inside the rock; due to the coupled effect of thermal treatment and repeated impacts, the higher energy levels contribute

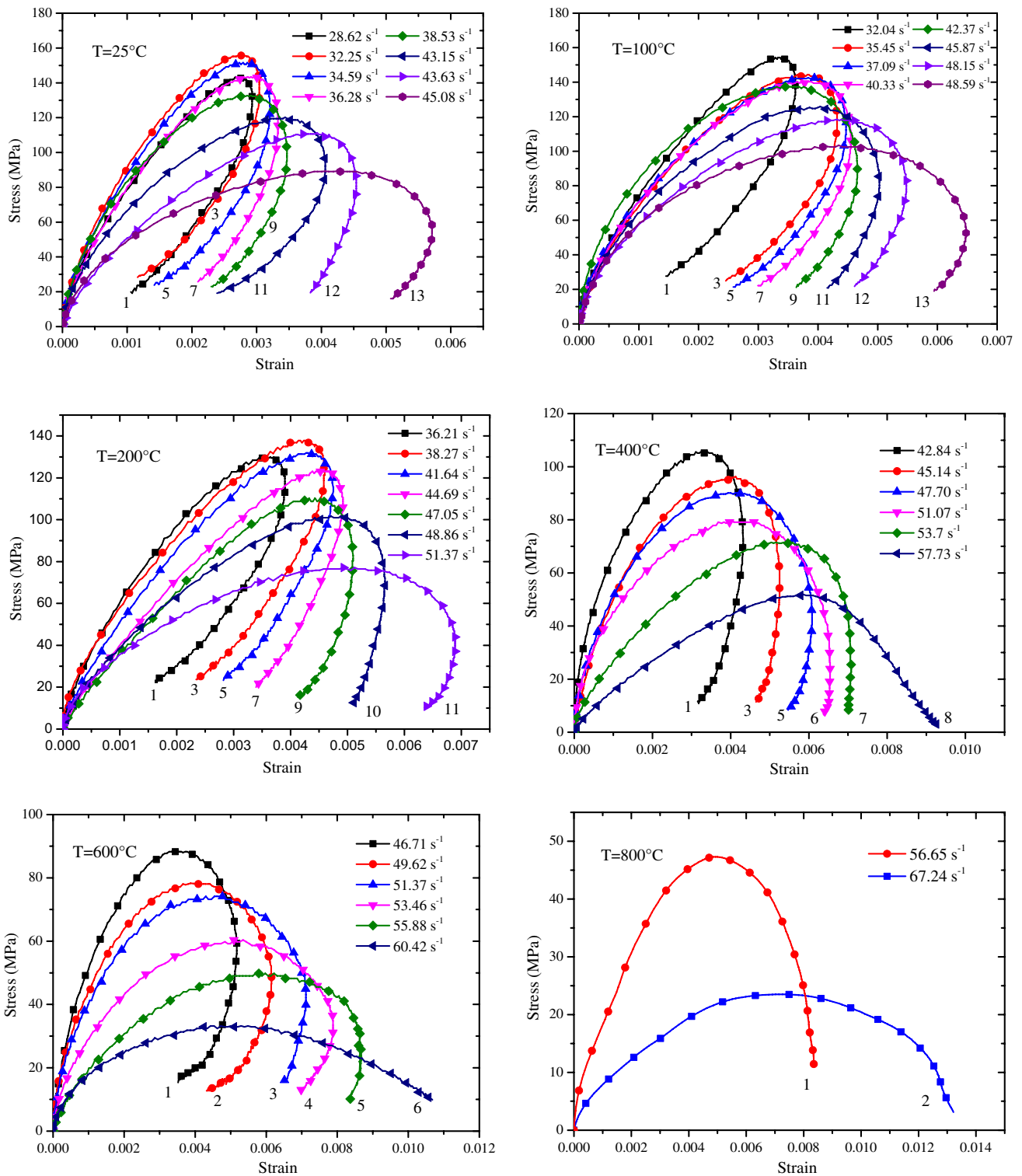


Fig. 15 Cyclic loading stress–strain curves for specimens treated at different temperatures

to extending these cracks, resulting in a sharp increase in damage and the granite no longer following the three-stage evolution process. In other words, the high-temperature effect aggravated the cumulative damage of the rock and

thus 400 °C can again be considered a threshold. Additionally, at all temperature stages, the cumulative damage is lower than 0.65 before the final impact, which suggests that this impact causes the sudden failure of the rock.

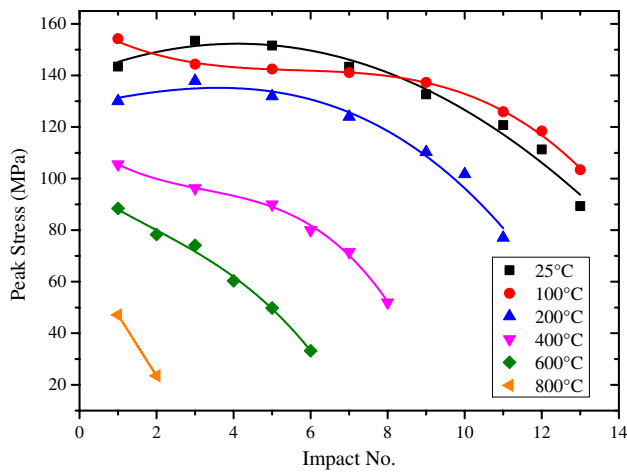


Fig. 16 Variation in compressive strength vs. cyclic impact number

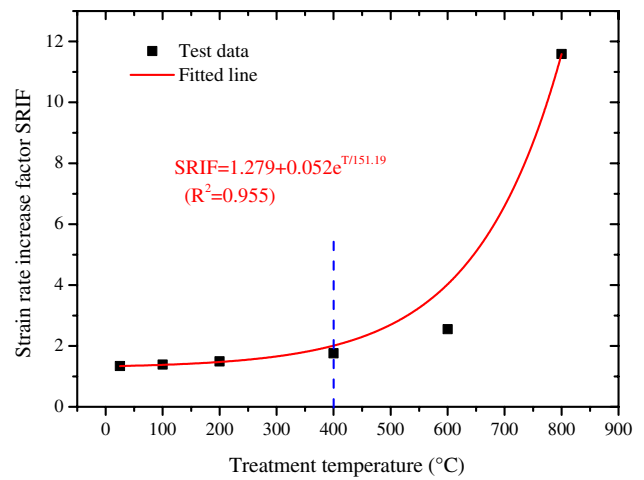


Fig. 18 Strain rate increase factor (SRIF) as a function of treatment temperature

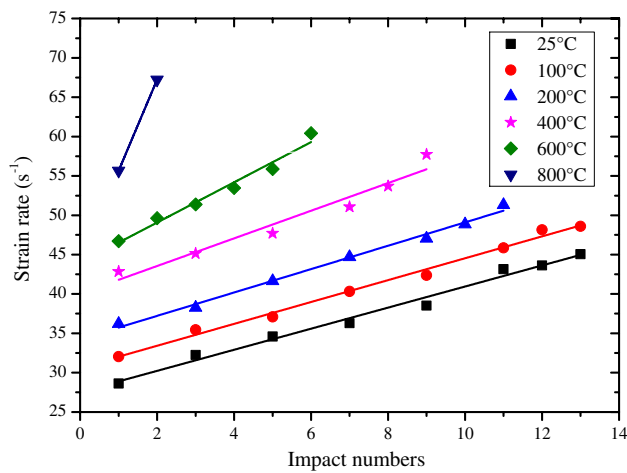


Fig. 17 Relationship between strain rate and repeated impact number

Table 3 Fitting equations for the strain rate as a function of the impact number

T (°C)	Relationship equation	R ²
25	$\dot{\epsilon} = 1.34 \times n + 27.55$	0.986
100	$\dot{\epsilon} = 1.39 \times n + 30.63$	0.991
200	$\dot{\epsilon} = 1.49 \times n + 34.24$	0.991
400	$\dot{\epsilon} = 1.76 \times n + 40.04$	0.938
600	$\dot{\epsilon} = 2.55 \times n + 43.97$	0.969
800	$\dot{\epsilon} = 11.59 \times n + 44.06$	—

However, this method of damage calculation has some disadvantages, such as that the initial thermal damage is not taken into account, and that the use of the maximum strain, as the sum of plastic strain and elastic strain, may have magnified the damage caused by cyclic loading.

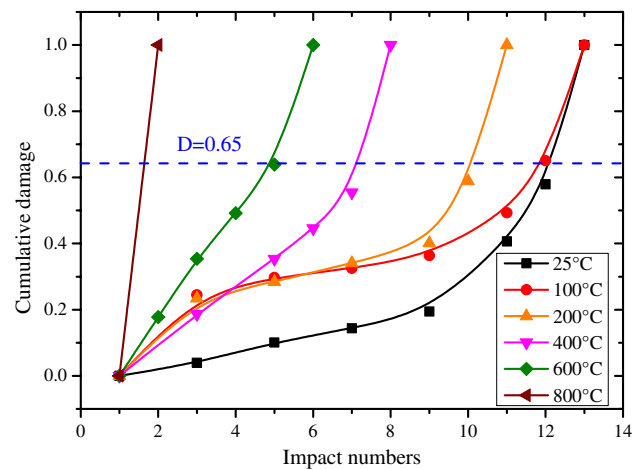


Fig. 19 Damage evolution of thermally treated granite described by maximum strain

4.4 Fatigue Life and Failure Modes

Under the same incident stress wave pattern, the granite rock samples withstood fewer and fewer impact cycles with increasing treatment temperature, which in turn indicates that thermal treatment resulted in considerable damage to the rock, as shown in Fig. 20. Although thermal treatment did not cause the appearance of macroscopic thermal cracking, at higher temperatures the internal thermal expansion of rock particles was more intense, activating potential micro-cracks. Griffith's theory of crack propagation states that when two different-length cracks are subjected to identical amplitude stress wave disturbances, the larger crack propagates faster than the small crack. Furthermore, the former can also easily exceed the fracture limit while absorbing

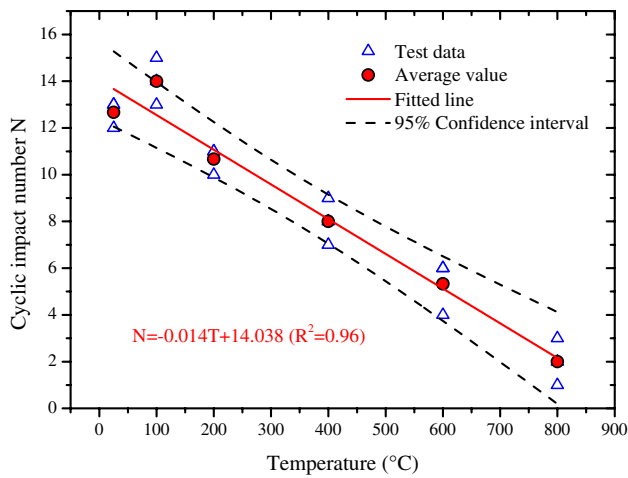


Fig. 20 Relationship between repeated impact number and treatment temperature

less energy or suffering fewer dynamic disturbances, which provides a good explanation as to why impact number was here negatively correlated with treatment temperature. Based on regression analysis, the relationship between repeated

impact numbers and temperature is expressed by the following equation:

$$n = - 0.0014T + 14.038 \quad R^2 = 0.96. \quad (9)$$

After each impact cycle, samples were photographed to study the fatigue damage evolution of the Changsha granite under coupled temperature and cyclic impact loading. Two representative samples after thermal treatment at 100 and 600 °C are presented in Fig. 21, which illustrates crack initiation and propagation (the right side of the specimen is the loading end). Each picture corresponds to a specific loading condition (impact number), with the final image in each row showing complete sample destruction. Figure 21a illustrates the development of cracks after thermal treatment at 100 °C. After eight impacts, debris had begun to flake off from the loading end of the specimen. After the subsequent impact, the damage zone was increased and a longitudinal crack parallel to the loading direction was generated. With an increase in repeated impacts, the initial crack gradually expanded and some secondary longitudinal cracks appeared on the sample surface as thin white lines. After 13 impacts, the rock sample was completely destroyed. As with the conventional dynamic tests, the broken fragments are strip-like in shape and their length is equal to the height of the specimen;

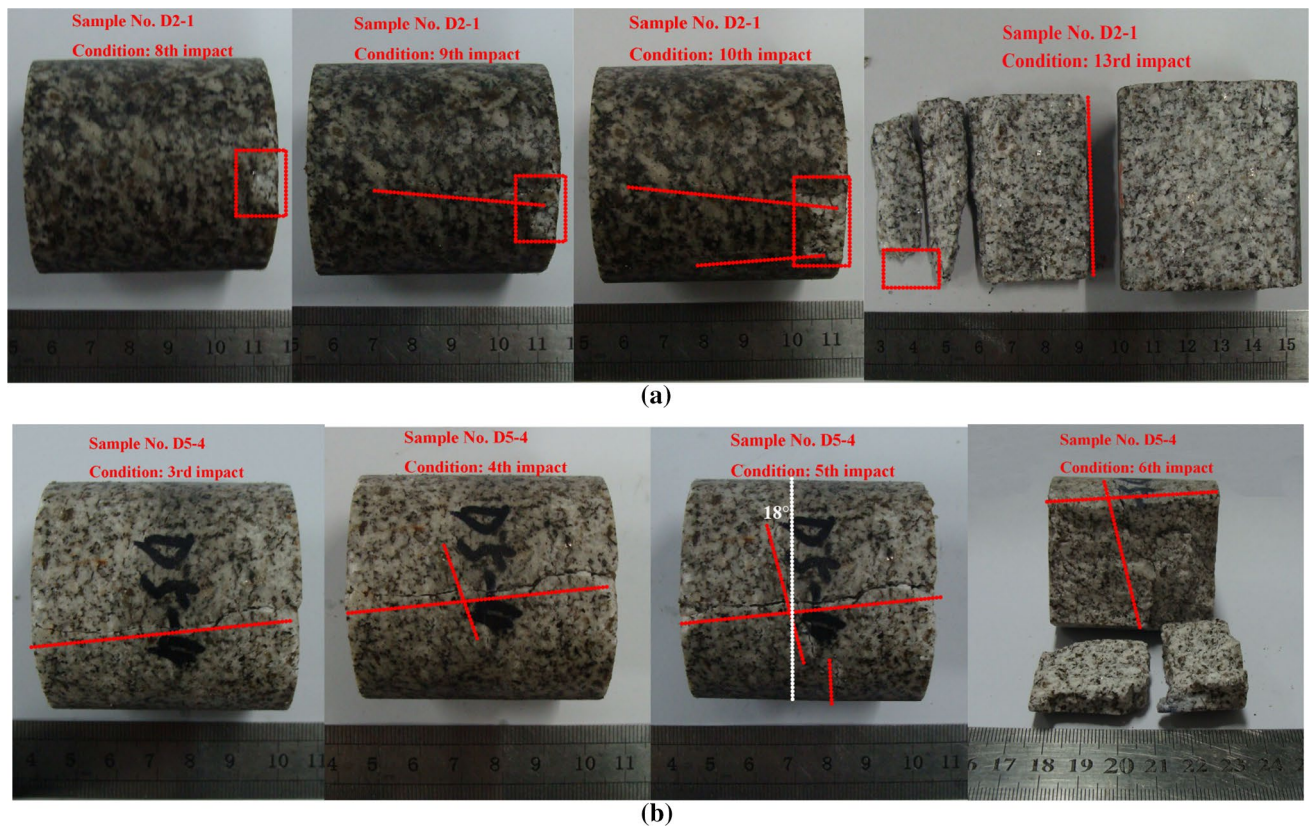


Fig. 21 Development of cracks on the surface of typical samples. **a** After thermal treatment at 100 °C; **b** after thermal treatment at 600 °C

the rupture surface is parallel to the longitudinal axis of the sample and no friction traces are apparent. Therefore, this type of fatigue damage can be considered splitting tensile damage, caused by the Poisson effect (Li et al. 2017).

In contrast, after high-temperature treatment at more than 600 °C, an obvious longitudinal crack appeared in the granite specimen after only three cycles of impact loading, as shown in Fig. 21b. Upon the 4th impact, a transverse crack approximately perpendicular to the axial direction of the specimen was observed, with the two orthogonal cracks gradually extending and crossing through each other by the fifth impact. Finally, after six impacts, a rare failure pattern was observed: one side of the sample split off and the whole specimen was vertically fractured into two sections approximately perpendicular to the axial direction. In fact, in all the conducted experiments, whereas at temperatures lower than 600 °C the samples presented split tensile fractures, at temperatures above 600 °C all samples presented this type of special fracture. Similar results were reported by Shan and Zhu (1998), and Li and Wang (1993), who refer to this damage mode as “unloading damage”. The latter authors also demonstrated that during dynamic loading, a great deal of strain energy is stored inside the rock, but during unloading these energies are released rapidly, resulting in expansion coaxial to the loading wave. Such expansion initially takes place at the two ends of the sample; hence, the unloading waves appear to diffuse from both ends towards the midsection. Finally, the sudden superposition of the two unloading waves leads to the abrupt fracture of the sample at the midsection. According to Li et al. (2003) and Tao and Zhang (2003), under low strain rate loading, a compression wave appears that is followed by the reflected tensile wave recorded in the incident bar, which indicates that energy release has occurred during the unloading process. However, the analyses of rock unloading damage were based only on the hypothesis of expansion motion, as during the process of damage accumulation in rocks under cyclic impact loading, the transverse crack is not completely perpendicular to the axial direction of the specimen, with an angle deviation of 18° (shown in Fig. 21b), indicating that the compression shear effect might be also involved in the whole failure process of the thermally treated rock. The relevant evidence for shear failure can also be obtained from the numerical study of Zhou et al. (2017a, b), they presented that shear cracks emerged first and stopped developing when the external stress was not high enough.

4.5 Microscopic Features of Granite Failure

Fracture failure of rock material under external load will produce different forms of fractography, which mainly depends on the internal structure of the rock and the loading magnitude and path of the external loads. External load

affects the change of microcosmic characteristics of rock by influencing the changes of micro-defects and microstructures in the rock. By SEM scanning analysis of rock failure fracture after loading, the process of rock fracture can be traced and the mechanism information of rock fracture can be extracted.

It could be observed from Fig. 22, when the temperature ranges from 25 to 400 °C, rock failure is characterized by typical brittle fracture characteristics. The fracture surface is smooth and the failure mode is mainly transgranular fracture with a less amount of intergranular failure can also be found in some local areas. The main reason causing this phenomenon might be that the transgranular fracture form needs to destroy the structure of the crystal itself, and the energy needed is obviously greater than the energy consumed by the intergranular fracture. Under the impact loading condition, the energy of the incident wave is relatively high and the energy rock absorbed is large, cracks inside rock do not have enough time to find the weakest surface of atomic bonding force, resulting in transgranular fractures. Along with the increase of treatment temperature, the characteristics of transgranular fracture are more obvious, and the intergranular crack size increases gradually. When the temperature exceeds 600 °C, the fracture surface of granite is rough and the failure path becomes more complex. A large number of transgranular fractures lead to small fragmentation of rock, and some rock debris was generated on the surface of fracture. The main reason causing this phenomenon might be that a large amount of transgranular damage has been produced inside the rock before loading, and some irreversible plastic deformation has also been produced by high-temperature treatment. Under the action of cyclic impact loading, the internal structure of the rock becomes more broken, and the broken crystals are rubbed with each other, resulting in a large amount of fatigue debris on the surface of the fracture.

5 Conclusion

In this study, a split Hopkinson pressure bar (SHPB) system and scanning electron microscopy (SEM) were employed to investigate the influence of damage induced by coupled thermal treatment and repeated impacts on Changsha granite. The results of this analysis indicated that higher temperatures cause some initial damage to the granite rock mass, with intergranular cracks and transgranular fractures appearing at 200 and 600 °C, respectively.

Under the coupled effect of thermal treatment and repeated impacts, the dynamic strength and deformation capacity of the granite degrade gradually and the rock undergoes a transformation from brittle to plastic. In addition, the dynamic strain rate increases continually with an increase in impact number, with its growth rate also exhibiting an

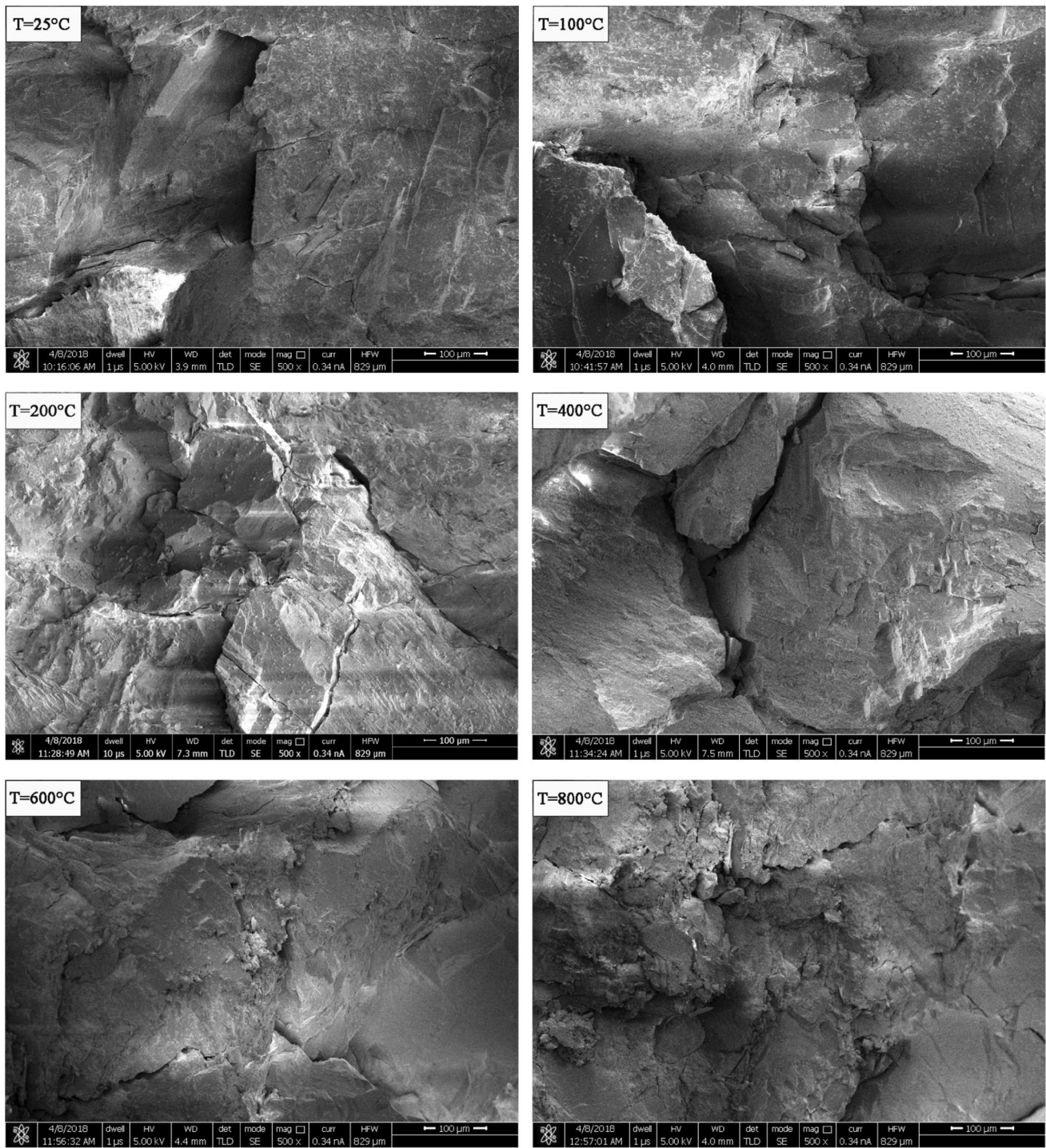


Fig. 22 Micro-properties of fracture morphology in the granite after loading

obvious temperature effect. The maximum strain of the rock under different temperatures and impact numbers was used as the damage variable to describe the damage evolution process after each impact. After treatment at relatively low temperatures (below 400 °C), damage evolution takes place in three distinct stages, including an initial stage, stable

development stage and sharp increase stage. However, when the treatment temperature exceeds 400 °C, the increase in damage is rapid and linear, and thus this temperature can be seen as an important threshold.

At increasingly high treatment temperatures, the rock samples can withstand fewer and fewer impact cycles. Two

different failure modes are exhibited: split tensile failure after treatment below 400 °C and unloading failure after treatment at 600 °C. The mechanisms of these two types of fatigue failure were discussed in detail from the point of view of energy unloading and expansion deformation. Microscopic fracture morphology of granite after different high temperatures and repeated impact loading was also analyzed. In results indicating that under lower temperature ranging from 25 to 400 °C, rock failure is characterized by typical brittle fracture characteristics. When the temperature exceeds 600 °C, the fracture surface of granite is rough and the failure path becomes more complex. A large number of transgranular fractures lead to small fragmentation of rock, and some rock debris was also generated on the surface of fracture. The main reason for the failure morphology is the combined effect of high temperature and fatigue load.

Acknowledgements The research presented in this paper was carried out under the jointly financial support of the National Natural Science Foundation of China (no. 51774325), State Key Research Development Program of China (no. 2016YFC0600706), the State Key Program of National Natural Science Foundation of China (no. 41630642) and Innovation-Driven Project of Central South University (no. 2017CX006). The authors would like to thank their colleagues of the Rock Mechanics and Blasting Engineering research group at the Central South University for technical discussion and comments. Also, the authors express their acknowledgements to the anonymous reviewers for their precious comments.

References

- Ackermann RJ, Sorrell CA (2010) Thermal expansion and the high-temperature transformation in quartz. I. High-temperature X-ray studies. *J Appl Crystallogr* 7(5):461–467
- Bagde MN, Petros V (2009) Fatigue and dynamic energy behavior of rock subjected to cyclical loading. *Int J Rock Mech Min Sci* 46:200–209
- Bagde MN, Petroš V (2005) Waveform effect on fatigue properties of intact sandstone in uniaxial cyclical loading. *Rock Mech Rock Eng* 38(3):169–196
- Behrmann JH, Mainprice D (1987) Deformation mechanisms in a high-temperature quartz-feldspar mylonite: evidence for superplastic flow in the lower continental crust. *Tectonophysics* 140(2):297–305
- Carroll J, Daly S (2015) *Fracture, fatigue, failure, and damage evolution*, vol 5. Springer, Dordrecht
- Chen R, Xia K, Dai F et al (2009) Determination of dynamic fracture parameters using a semi-circular bend technique in split Hopkinson pressure bar testing. *Eng Fract Mech* 76(9):1268–1276
- Das R, Sirdesai N, Singh T (2017) Analysis of deformational behavior of circular underground opening in soft ground using three-dimensional physical model. In: 51st US rock mechanics/geomechanics symposium, San Francisco, California, USA. American Rock Mechanics Association
- Dwivedi RD, Goel RK, Prasad VVR et al (2008) Thermo-mechanical properties of Indian and other granites. *Int J Rock Mech Min Sci* 45(3):303–315
- Fan LF, Wu ZJ, Wan Z et al (2017) Experimental investigation of thermal effects on dynamic behavior of granite. *Appl Therm Eng* 125:94–103
- Franklin JA, Vogler UW, Szlavín J, Edmond JM, Bieniawski ZT (1979) Suggested methods for determining water content, porosity, density, absorption and related properties and swelling and slake-durability index properties: Part 1: suggested methods for determining water content, porosity, density, absorption and related properties. *Int J Rock Mech Min Sci Geomech Abstr* 16(2):143–151
- Ge X, Jiang Y, Lu Y et al (2003) Experimental study on fatigue deformation law of rock under cyclic loading. *J Rock Mech Eng* 22(10):1581–1581
- Grim RE, Kulbicki G (1961) Montmorillonite: high temperature reactions and classification. *Am Miner* 46:1329–1369
- Hajpál M, Török Á. (2004) Mineralogical and colour changes of quartz sandstones by heat. *Environ Geol* 46(3–4):311–322
- Heuze FE (1983) High-temperature mechanical, physical and thermal properties of granitic rocks—a review. *Int J Rock Mech Min Sci Geomech Abstr* 20(1):3–10
- Homand-Etienne F, Houpert R (1989) Thermally induced microcracking in granites: characterization and analysis. *Int J Rock Mech Min Sci Geomech Abstr* 26(2):125–134
- ISRM (1978) Commission on standardization of laboratory and field tests of the international society for rock mechanics: “suggested methods for the quantitative description of discontinuities”. *Int J Rock Mech Min Sci* 15(6):320–368
- Jin J, Li X, Wang G, Yin Z (2012) Failure modes and mechanisms of sandstone under cyclic impact loadings. *J Cent South Univ* 43(4):1453–1461
- Karfakis MG, Akram M (1993) Effects of chemical solutions on rock fracturing. *Int J Rock Mech Min Sci Geomech Abstr* 30(7):1253–1259
- Lai JZ, Sun W (2010) Dynamic damage and stress–strain relations of ultra-high performance cementitious composites subjected to repeated impact. *Sci China Technol Sci* 53(6):1520–1525
- Lajtai EZ (1971) A theoretical and experimental evaluation of the Griffith theory of brittle fracture. *Tectonophysics* 11(2):129–156
- Li T, Wang L (1993) An experimental study on the deformation and failure features of a blast under unloading condition. *J Rock Mech Eng* 12(4):321–327
- Li XB, Lok TS, Zhao J et al (2000) Oscillation elimination in the Hopkinson bar apparatus and resultant complete dynamic stress–strain curves for rocks. *Int J Rock Mech Min Sci* 37(7):1055–1060
- Li N, Zhang P, Chen YS, Swoboda G (2003) Fatigue properties of cracked, saturated and frozen sandstone samples under cyclic loading. *Int J Rock Mech Min Sci* 40(1):145–150
- Li XB, Lok TS, Zhao J (2005) Dynamic characteristics of granite subjected to intermediate loading rate. *Rock Mech Rock Eng* 38(1):21–39
- Li X, Zou Y, Zhou Z (2014) Numerical simulation of the rock SHPB test with a special shape striker based on the discrete element method. *Rock Mech Rock Eng* 47(5):1693–1709
- Li X, Gong F, Tao M et al (2017) Failure mechanism and coupled static–dynamic loading theory in deep hard rock mining: a review. *J Rock Mech Geotech Eng* 9:767–782
- Lima JJDC, Paraguassú AB (2004) Linear thermal expansion of granitic rocks: influence of apparent porosity, grain size and quartz content. *Bull Eng Geol Environ* 63(3):215–220
- Liu E, He S (2012) Effects of cyclic dynamic loading on the mechanical properties of intact rock samples under confining pressure conditions. *Eng Geol* 125(1):81–91
- Liu S, Xu J (2013) Study on dynamic characteristics of marble under impact loading and high temperature. *Int J Rock Mech Min Sci* 62(5):51–58
- Liu S, Xu J (2015) An experimental study on the physico-mechanical properties of two post-high-temperature rocks. *Eng Geol* 185(4):63–70

- Liu J, Xie H, Hou Z et al (2014) Damage evolution of rock salt under cyclic loading in uniaxial tests. *Acta Geotech* 9(1):153–160
- Luo X, Jiang N, Wang M et al (2015) Response of leptynite subjected to repeated impact loading. *Rock Mech Rock Eng* 49:1–5
- Nasseri MHB, Schubnel A, Young RP (2007) Coupled evolutions of fracture toughness and elastic wave velocities at high crack density in thermally treated Westerly granite. *Int J Rock Mech Min Sci* 44(4):601–616
- Peng Z, Redfern SAT (2013) Mechanical properties of quartz at the α - β phase transition: implications for tectonic and seismic anomalies. *Geochem Geophys Geosyst* 14(1):18–28
- Ranjith PG, Viete DR, Chen BJ et al (2012) Transformation plasticity and the effect of temperature on the mechanical behaviour of Hawkesbury sandstone at atmospheric pressure. *Eng Geol* 151(151):120–127
- Ray SK, Sarkar M, Singh TN (1999) Effect of cyclic loading and strain rate on the mechanical behaviour of sandstone. *Int J Rock Mech Min Sci* 36(4):543–549
- Roddy DJ, Younger PL (2010) Underground coal gasification with CCS: a pathway to decarbonising industry. *Energy Environ Sci* 3(4):400–407
- Schaefer L, Kendrick J, Lavallée Y et al (2015) Geomechanical rock properties of a basaltic volcano. *Front Earth Sci* 3(29):29
- Shan R, Zhu Z (1998) A study on the impact failure pattern of marble and granite. *J Rock Mech Eng* 17(Suppl.):774–779
- Shan R, Jiang Y, Li B (2000) Obtaining dynamic complete stress–strain curves for rock using the Split Hopkinson Pressure Bar technique. *Int J Rock Mech Min Sci* 37(6):983–992
- Sun B, Zhu Z, Shi C et al (2017) Dynamic mechanical behavior and fatigue damage evolution of sandstone under cyclic loading. *Int J Rock Mech Min Sci* 94:82–89
- Tao J, Zhang F et al (2003) An experimental method for studying dynamic unloading property of material. *Explos Shock* 23(5):436–441
- Tian H, Ziegler M, Kempka T (2014) Physical and mechanical behavior of claystone exposed to temperatures up to 1000 °C. *Int J Rock Mech Min Sci* 70:144–153
- Tian H, Mei G, Jiang GS et al (2017) High-temperature influence on mechanical properties of diorite. *Rock Mech Rock Eng* 50(6):1–6
- Wang ZL, Zhu HH, Wang JG (2013) Repeated-impact response of ultrashort steel fiber reinforced concrete. *Exp Tech* 37(4):6–13
- Wu B, Kanopoulos P, Luo X et al (2014) An experimental method to quantify the impact fatigue behavior of rocks[J]. *Meas Sci Technol* 25(7):075002
- Xiao JQ, Ding DX, Xu G et al (2009) Inverted S-shaped model for nonlinear fatigue damage of rock. *Int J Rock Mech Min Sci* 46(3):643–648
- Xiao JQ, Ding DX, Jiang FL et al (2010) Fatigue damage variable and evolution of rock subjected to cyclic loading. *Int J Rock Mech Min Sci* 47(3):461–468
- Yao W, Xu Y, Wang W et al (2016) Dependence of dynamic tensile strength of Longyou sandstone on heat-treatment temperature and loading rate. *Rock Mech Rock Eng* 49(10):1–17
- Yin T, Li X, Xia K et al (2012) Effect of thermal treatment on the dynamic fracture toughness of Laurentian Granite. *Rock Mech Rock Eng* 45(6):1087–1094
- Yin T, Li X, Cao W et al (2015) Effects of thermal treatment on tensile strength of Laurentian Granite using Brazilian test. *Rock Mech Rock Eng* 48(6):2213–2223
- Yin T, Wang P, Li X et al (2016) Determination of dynamic flexural tensile strength of thermally treated Laurentian Granite using semi-circular specimens. *Rock Mech Rock Eng* 49:3887–3898
- Yin T, Bai L, Li X et al (2018) Effect of thermal treatment on the mode I fracture toughness of granite under dynamic and static coupling load. *Eng Fract Mech* 199:143–158
- Zhang QB, Zhao J (2014) A review of dynamic experimental techniques and mechanical behaviour of rock materials. *Rock Mech Rock Eng* 47(4):1411–1478
- Zhang ZX, Yu J, Kou SQ et al (2001) Effects of high temperatures on dynamic rock fracture. *Int J Rock Mech Min Sci* 38(2):211–225
- Zhao Z (2016) Thermal influence on mechanical properties of granite: a microcracking perspective. *Rock Mech Rock Eng* 49(3):747–762
- Zhao J, Li HB (2000) Experimental determination of dynamic tensile properties of a granite. *Int J Rock Mech Min Sci* 37(5):861–866
- Zhou Z, Li X, Liu A et al (2011) Stress uniformity of split Hopkinson pressure bar under half-sine wave loads. *Int J Rock Mech Min Sci* 48(4):697–701
- Zhou YX, Xia K, Li XB et al (2012) Suggested methods for determining the dynamic strength parameters and mode-I fracture toughness of rock materials. *Int J Rock Mech Min Sci* 49(1):105–112
- Zhou Z, Jiang Y, Zou Y et al (2014) Degradation mechanism of rock under impact loadings by integrated investigation on crack and damage development. *J Cent South Univ* 21(12):4646–4652
- Zhou Z, Cai X, Chen L et al (2017a) Influence of cyclic wetting and drying on physical and dynamic compressive properties of sandstone. *Eng Geol* 220:1–12
- Zhou Z, Zhao Y, Jiang Y et al (2017b) Dynamic behavior of rock during its post failure stage in SHPB tests. *Trans Nonferrous Metals Soc China* 27(1):184–196

Publisher's Note Springer Nature remains neutral with regard to jurisdictional claims in published maps and institutional affiliations.